Fuel 241 (2019) 1036–1044

Contents lists available at ScienceDirect

Fuel

journal homepage: www.elsevier.com/locate/fuel

Full Length Article

Porosity and storage capacity of Middle Devonian shale: A function of thermal maturity, total organic carbon, and clay content

Liaosha Song[a,b,*], Keithan Martin[b], Timothy R. Carr[b], Payam Kavousi Ghahfarokhi[b]

[a] Department of Geological Sciences, California State University, Bakersfield, CA 93311, USA
[b] Department of Geology and Geography, West Virginia University, Morgantown, WV 26506, USA

ARTICLE INFO

Keywords:
Porosity
Pore size distribution
Marcellus Shale
Pore structure
Storage capacity
Shale gas reservoirs

ABSTRACT

Porosity and pore size distribution (PSD) are critical reservoir parameters. Pore surface area, pore volume, PSD, and porosity were measured using subcritical nitrogen (N_2) adsorption, and helium porosimetry. A suite of 17 samples were collected from 4 wells in Pennsylvania and West Virginia to analyze the evolution of porosity with increasing thermal maturity in Middle Devonian shales of the Appalachian Basin. The thermal maturity of the tested samples covers a wide range in the hydrocarbon generation sequence from wet gas/condensate zone (vitrinite reflectance (R_o) = 1.16%) to post-mature zone (R_o = 2.79%). Shale samples from the Marcellus Shale and Mahantango Formation used in this study have total organic carbon contents from 0.41 to 7.88 wt%. Results indicate that total organic carbon (TOC) has the strongest effect on porosity and pore structure. The presence of organic matter in shale strongly enhances the storage capacity by increasing the specific surface area and pore volume, which represents sorption storage capacity and free-gas storage capacity. Differences in porosity and pore structure have a complex relationship to thermal maturity, micro texture, mineralogy, clay content, and TOC.

1. Introduction

The performance of a shale reservoir critically depends on the pore systems since they provide the storage capacity and pathway for hydrocarbon flow. Porosity and pore size distribution are widely used to characterize pore structure [1–5].The pore-throat size in shale reservoirs ranges from submicron to nanometer scale [6], which is significantly smaller than that of conventional reservoirs. Also, the pore systems in shale reservoirs are composed of pores hosted by both mineral grains and organic matter, and fractures. As a result, a variety of pore sizes and fluid flow regime occur in shales, from Darcy flow in large connected pores to slippage and Knudsen diffusion in nanometer-scale organic matter (OM) hosted pores [7–9]. The heterogeneity of fine-grained strata and the wide distribution of pore sizes make it challenging to evaluate a shale reservoir. Many geologic factors, including total organic carbon (TOC), mineralogy, thermal maturity, and grain assemblage, have been investigated to determine their influence of pore structure [10–14].

The Appalachian Basin is a foreland basin that formed as a result of numerous successive orogenies along the southeast margin of Ancestral North America throughout the Neoproterozoic to the Late Triassic [15]. Several shale units were deposited throughout the history of the basin, although the Hamilton Group, due to lateral continuity, organic-richness, and vast hydrocarbon potential, has been the focal point of study over the last two decades. The Hamilton Group is largely made up of two mudrock formations, namely the organic-rich Marcellus Shale (basal unit) and the organic-lean Mahantango Formation [16]. The Hamilton Group units were deposited as a part of the Catskill Delta complex, which is a wedge of clastic marine and terrestrial deposits sourced from the highlands of the northern margin of the basin [17–22]. The Marcellus shale was deposited under anoxic to euxinic conditions with limited siliciclastic influx, resulting in the preservation of large quantities of organic matter, giving the Marcellus Shale the distinct dark-gray to black appearance in core and outcrop [23]. In contrast, the Mahantango Formation was deposited under oxic to dysoxic conditions, with considerable amount siliciclastic influx from northern highlands, which created a more diluted, relatively organic-lean grey to dark grey mudrock. Due to these characteristics, the Marcellus Shale was considered as the chief source-rock formation during the early development of gas plays in the Appalachian basin during 1930s–1960s [24]. The study of the Marcellus Shale as a target reservoir started with the Eastern Gas Shales Project funded by the US Department of Energy during late 1970s through the 1980s [24,25]. Early studies of the porosity and permeability of the Middle Devonian

* Corresponding author.
E-mail address: lsong1@csub.edu (L. Song).

https://doi.org/10.1016/j.fuel.2018.12.106
Received 17 June 2018; Received in revised form 18 December 2018; Accepted 21 December 2018
Available online 31 December 2018

shale succession revealed that organic matter content and thermal maturity influence the potential productivity [26–28]. The introduction of horizontal drilling and hydraulic fracturing techniques enabled the economic production of a series of shale reservoirs including the Marcellus Shale [24,25].

Organic matter hosted porosity has been considered as the dominant gas storage capacity of shale residue in the kerogen network [14,29]. Milliken et al. (2013) studied a set of samples at a thermal maturity between an Ro of 1.0 and 2.1% in the Marcellus Shale of northern Pennsylvania, and found that variation of TOC is a stronger control on the character of OM-hosted pore systems than variation in thermal maturity, especially at TOC contents < 5.6 wt% [30]. Gu et al. (2015) investigated the porosity of Marcellus Shale from a core drilled in Centre County, Pennsylvania, USA, using ultra small-angle neutron scattering (USANS), small-angle neutron scattering (SANS), FIB-SEM, and nitrogen gas adsorption. They argue that the dominant nanometer sized pores in organic-poor, clay-rich shale samples are water-accessible sheet-like pores within clay aggregates. In contrast, bubble-like organophilic pores in kerogen dominate organic-rich sample [31].

Numerous studies about the evolution of OM hosted porosity with thermal maturation have been conducted with different methodologies, yet this question is still not well understood. Although OM-hosted porosity is created during thermal cracking of kerogen and generation of hydrocarbon [32–34], maturity alone is not a reliable predictor of porosity in organic matter, and other factors such as the composition of OM could also influence the generation of organic matter hosted porosity. Curtis et al. (2011) analyzed two Marcellus Shale samples with vitrinite reflectance of 1.1% and over 3.1%, using focused ion beam (FIB) milling and scanning electron microscopy (SEM). They found no correlation between thermal maturity and OM hosted porosity [35]. Mechanical compaction is also an important factor when evaluating the preservation of OM-hosted porosity, since OM is normally less resistant towards mechanical compaction compared with the rest of the rock [36]. Mastalerz et al. (2013) examined five New Albany Shale samples with a maturity range from immature to post mature and emphasized the importance of mineralogical composition to porosity. They conclude that hydrocarbon generation and migration is the main reason of the changes observed in porosity and pore volume [7]. Given the number of geologic factors controlling the generation and modification of OM-hosted pores, a systematic study of porosity and storage capacity evolution through thermal maturation is in need.

In this study, we selected a suite of core samples from the Mahantango Formation and the Marcellus Shale covering a range from wet gas (Ro 1.16%) to post-mature (Ro 2.79%). The focus of this study is to better understand the effects of thermal maturity on evolution of porosity and storage capacity.

2. Materials and methods

2.1. Materials

Seventeen core samples were collected from 4 wells penetrating Marcellus and Mahantango shales in West Virginia and Pennsylvania (Figs. 1 and 2). Table 1 lists the samples analyzed in this research, including the formations from which they were sampled, TOC, and thermal maturity (represented by vitrinite reflectance, R_o). Four samples were taken from the CS1 well, located in Clearfield County, Pennsylvania, four samples were taken from the SW1 well, located in Greene County, Pennsylvania, three samples were taken from the G55 well, located in Harrison County, West Virginia, and five samples were taken from the A1well, located in Taylor County, West Virginia. The mudrock samples were selected to cover a range of thermal maturities from a Ro of 1.16% to 2.79%, which represents a range from the condensate zone to the post-mature zone. Some samples are from the same wells and depths as the samples that were studied extensively in previous research at the Department of Geology and Geography, West Virginia University [37–41]. This helped us during the selection of samples in this research. Samples represent a wide range of mineralogical composition and organic-matter content, and represent the Marcellus Shale and Mahantango Formation relatively well.

2.2. Subcritical nitrogen adsorption

Subcritical N_2 adsorption was conducted on a Micromeritics ASAP-2020 instrument at −196 °C (77 K). About 1 g of shale sample was crushed with mortar and pestle until the whole mass passes through a 60-mesh sieve to prevent potential sample biasing due to sieving. Then samples were set under high-vacuum at 120 °C for 24 h to remove adsorbed water and volatile matter prior to analyses with N_2. Forty-three relative-pressure (P/P0) points ranging from 0.009 to 0.990 were measured on both adsorption and desorption branches. The adsorption branch of the isotherms from samples was used to obtain information about micropores (< 2 nm in diameter) and mesopores (2–50 nm in diameter). The classification of pore sizes used in this article follows the classification system of the International Union of Pure and Applied Chemistry. This classification of pore sizes has proven to be very convenient in coal and shale studies [1,7,11,42]. Specific surface area (SSA) was calculated based on Brunauer-Emmet-Teller (BET) theory [43]. Pore volumes and pore distributions are based on Barrett-Joyner-Halenda (BJH) model, t-Plot, H-K model [43–45]. A detailed description of these theories and techniques can be found in *Reporting Physisorption Data for Gas/Solid Systems*, and *Physisorption of Gases, with Special Reference to the Evaluation of Surface Area and Pore Size Distribution* [46,47].

2.3. Porosity

Porosity was measured using the Gas Research Institute (GRI) helium porosimetry method on crushed core samples [28], and was conducted by Core Laboratories in Houston, Texas. The bulk volume is determined by Archimedes' principle with mercury immersion, and grain volume is determined using Boyle's Law with helium expansion. Pore fluids were removed by Dean Stark extraction, and crushed samples (20–35 mesh) were dried at 110 °C. Porosity is calculated based on the difference between bulk volume and grain volume.

2.4. Mineralogical composition

Mineralogical composition was quantified with X-ray Diffraction (XRD). The samples were ground in a steel grinding container to ultrafine particle size and pressed into chemplex pellets. XRD was performed with a PANalytical X'Pert Pro X-ray Diffractometer at the Shared Research Facilities of West Virginia University. The original spectra were interpreted using the X'Pert HighScore Plus Program.

2.5. Additional data

Total organic carbon is determined with approximately 60–100 mg of pulverized mudrock sample in the Source Rock Analyzer (SRA) at the National Energy Technology Laboratory (NETL). Vitrinite reflectance was provided by Core Laboratories in Houston, TX as shared in part with a joint industry project, the Marcellus Shale Consortium.

3. Results

3.1. Mineralogy, total organic carbon, and porosity

Results of XRD analysis for this sample suite demonstrate a very wide distribution in mineralogy (Table 2 and Fig. 3). Quartz and clay minerals are the major constituents in most of the samples. Sample CS1-2 was also taken from a carbonate rich layer, which contains 36.8% carbonate (calcite and dolomite). Clay minerals specifically illite and

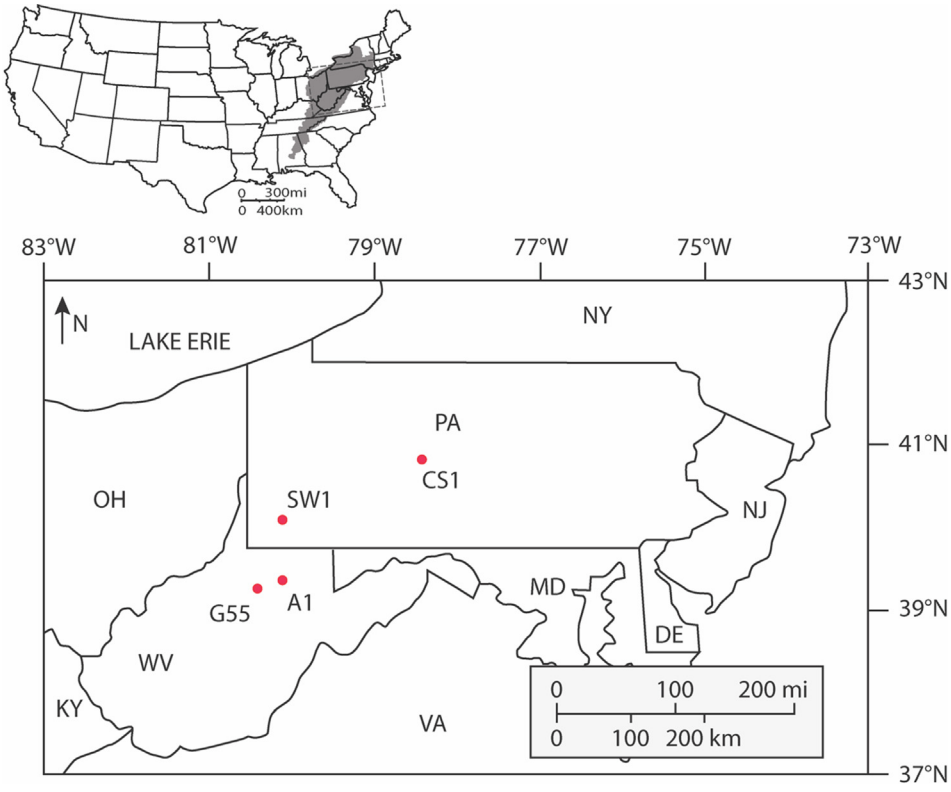

Fig. 1. Locations of the four study wells.

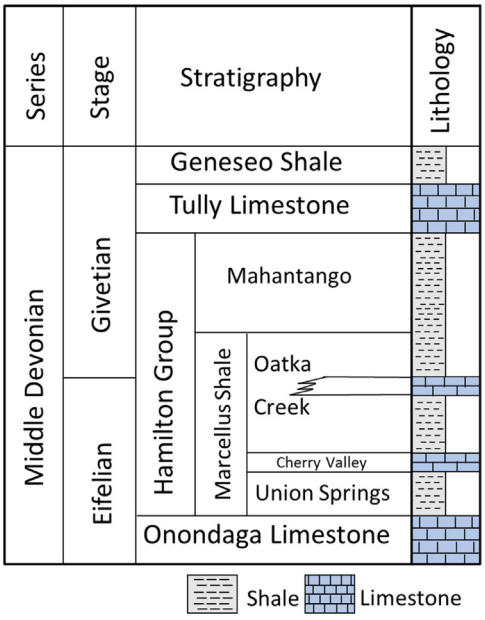

Fig. 2. Stratigraphy of the study area.

chlorite, are dominant in most of the Mahantango samples (G55-1, A1-1, A1-2, CS1-1, and SW1-1). Sample A1-2 from the lower part of Mahantango Formation illustrates nearly equal percentages of quartz and total clay, 46.6% and 40.5% respectively. The relative abundance of individual clay minerals also varies in different samples. In samples from well G55, A1, and SW1, illite and mica exceeded chlorite, whereas in well CS1 chlorite is the major clay mineral. Samples G55-3, A1-4, SW1-1, and SW1-2 show no chlorite, while sample CS1-4 with a similar organic content level with the previous mentioned four samples shows 30.6% chlorite.

Table 1
Vitrinite reflectance (Ro), total organic carbon (TOC) content, depth, and formation of shale samples.

Sample name	Well #	Depth (ft)	Formation	TOC (wt.%)	R_o (%)
G55-1	G55	7099.00	Mahantango	0.65	1.36
G55-2	G55	7149.50	Marcellus	4.28	1.36
G55-3	G55	7211.00	Marcellus	5.91	NA
A1-1	A1	7555.00	Mahantango	2.10	1.40
A1-2	A1	7605.00	Mahantango	2.24	1.38
A1-3	A1	7714.00	Marcellus	4.34	1.46
A1-4	A1	7734.00	Marcellus	5.84	NA
A1-5	A1	7765.00	Marcellus	5.12	1.41
CS1-1	CS1	7019.00	Mahantango	1.80	2.59
CS1-2	CS1	7070.00	Marcellus	2.33	2.67
CS1-3	CS1	7099.50	Marcellus	7.28	2.68
CS1-4	CS1	7128.00	Marcellus	4.28	2.79
CS1-5	CS1	7145.00	Marcellus	6.20	NA
SW1-1	WS1	7742.00	Mahantango	0.41	1.25
SW1-2	WS1	7852.00	Marcellus	4.66	1.16
SW1-3	WS1	7873.00	Marcellus	4.80	1.18
SW1-4	WS1	7891.00	Marcellus	7.88	NA

Total organic carbon ranges from 1.94% to 7.88% in samples from the Marcellus Shale. While in Mahantango Formation, it ranges from 0.41% to 2.24%. Generally, the TOC of Marcellus Shale is significantly higher than Manhantango Formation, and that of lower Marcellus (Union Springs Member) is higher than the upper Marcellus (Oakta Creek Member).

Helium porosimetry was employed to provide comparative values for grain density, bulk sample density, and total porosity (Table 3). The porosity ranges from 1.95% for sample A1-2 to 7.56% for sample G55-2.

3.2. Nitrogen adsorption

N_2 adsorption at −196 °C is used to investigate pore volume and

Table 2
Mineralogy Composition of Shale Samples in Volume Percentage.

Sample #	Quartz	K-Feldspar	Plagioclase	Calcite	Dolomite	Pyrite	Kerogen	Illite & Mica	Chlorite
G55-1	36.3	0.6	5.0	3.9	0.7	0.5	1.5	33.2	18.4
G55-2	47.4	0.0	3.1	1.9	0.0	3.3	9.5	27.6	7.1
G55-3	49.8	0.0	3.0	10.1	0.0	3.9	12.9	20.3	0.0
A1-1	37.3	0.7	5.5	0.0	0.0	2.4	4.8	33.8	15.5
A1-2	46.2	0.0	4.4	0.7	0.0	2.9	5.1	27.7	12.8
A1-3	33.1	0.0	4.1	5.5	1.9	8.4	10.0	37.0	0.0
A1-3	53.3	0.0	2.9	1.7	1.4	4.1	12.8	23.9	0.0
A1-4	57.8	0.0	2.2	3.3	1.6	5.9	11.5	17.8	0.0
CS1-1	37.8	0.7	5.4	0.3	0.8	0.6	4.1	18.4	32.1
CS1-2	24.8	0.5	2.5	32.0	3.4	2.7	5.3	9.1	19.7
CS1-3	29.9	0.5	4.8	0.5	0.3	5.8	16.0	10.7	31.5
CS1-4	32.9	0.0	4.0	11.7	1.5	6.9	10.0	7.5	25.5
CS1-5	35.1	0.6	4.5	2.3	0.8	4.6	13.8	7.8	30.6
SW1-1	37.1	1.5	5.7	4.0	2.6	0.3	0.6	35.4	12.8
SW1-2	41.9	0.7	4.7	2.3	1.5	4.3	10.4	31.1	3.1
SW1-3	35.9	1.1	5.9	8.3	0.6	8.8	11.1	28.3	0.0
SW1-4	49.4	0.6	3.2	11.4	0.9	6.0	17.2	11.3	0.0

pore surface area. Both adsorption and desorption branches were collected, and the adsorption branch is used for calculating the surface area and pore volume. All samples exhibit similar isotherm and hysteresis loops (Fig. 4). All the isotherms are classified as type IV with hysteresis loops according to IUPAC classification, indicating the existence of meso-porosity and slit-shape pores [47,48]. Among all the samples, Marcellus samples show better capability of adsorbing nitrogen than Mahantango samples (Fig. 4). Sample A1-4 exhibits the highest capacity of nitrogen adsorption. According to IUPAC, 1985, the N_2 adsorption isotherms of all the samples are type IV with type H4 hysteresis (Fig. 4). The presence of a hysteresis loops is usually attributed to capillary condensation in mesopore structures (2 nm < Pore Size < 50 nm) [45–48], which in this case indicates the existence of mesopores in shale reservoir. Moreover, the H4 hysteresis loops are mainly associated with narrow slit-like pores which have both meso-porosity and microporosity [46].

Brunauer-Emmett-Teller specific surface area (SSA), BJH pore volume, t-plot pore volume, BJH pore diameter, and average pore width are calculated from N_2 adsorption analysis (Table 4), and the results show a wide range of distribution. The average SSA and BJH pore volume of the Marcellus is 29.63 m^2/g and 0.032 cm^3/g, respectively,

Table 3
Bulk density, grain density, and GRI porosity of shale samples.

Sample #	Bulk Density (g/cm^3)	Grain Density (g/cm^3)	GRI Porosity (%)
G55-1	2.65	2.75	4.33
G55-2	2.48	2.66	7.56
G55-3	2.39	2.56	7.32
A1-1	2.66	2.77	4.66
A1-2	2.70	2.74	1.95
A1-3	2.52	2.69	7.00
A1-4	2.47	2.61	6.06
A1-5	2.46	2.60	6.04
CS1-1	2.63	2.77	6.06
CS1-2	2.62	2.75	5.77
CS1-3	2.59	2.83	9.32
CS1-4	2.60	2.76	6.97
CS1-5	2.61	2.73	5.92
SW1-1	2.70	2.78	3.61
SW1-2	2.55	2.68	5.77
SW1-3	2.53	2.67	6.22
SW1-4	2.45	2.63	7.41

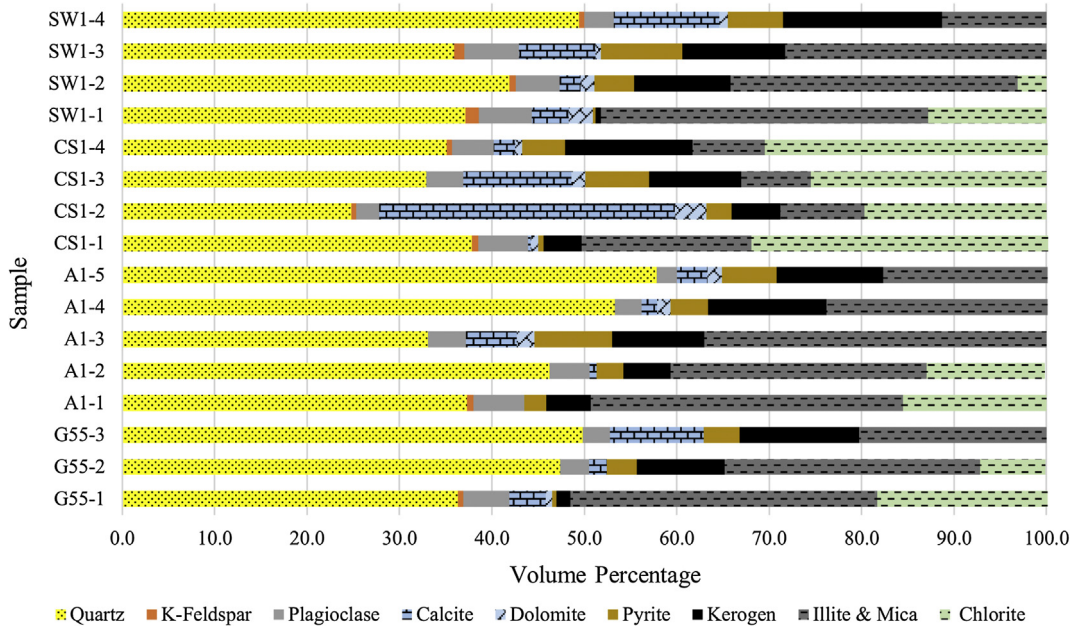

Fig. 3. Mineralogical composition of shale samples in volume percentage, data from Table 2.

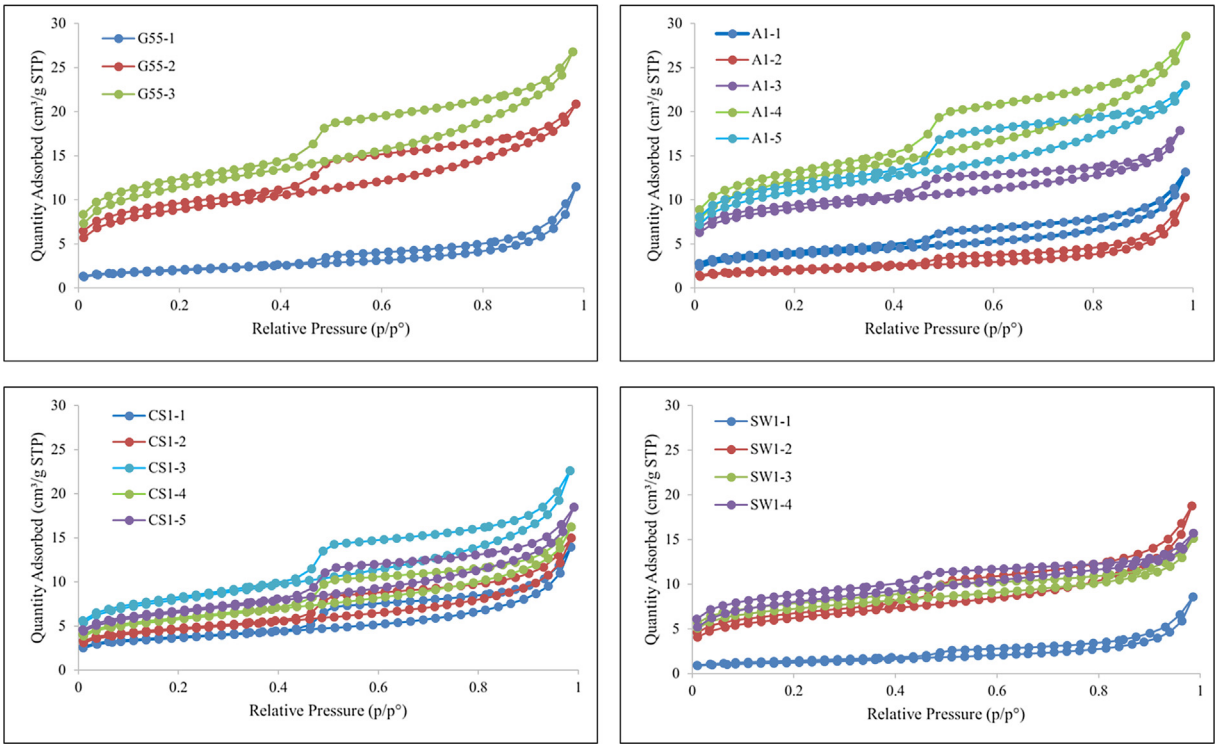

Fig. 4. Nitrogen adsorption isotherms of samples.

Table 4
Pore structure parameters determined via N_2 adsorption, in which, S_{BET} is BET SSA, V_{BJH} is BJH pore volume, and $V_{t\text{-}plot}$ is micropore volume calculated by t-plot method.

Sample	S_{BET} (m^2/g)	V_{BJH} (cm^3/g)	$V_{t\text{-}plot}$ (cm^3/g)	Average pore width (nm)	Median Pore Size (nm)
G55-1	7.0648	0.0181	0.0003	10.0809	37.1455
G55-2	31.8860	0.0313	0.0026	4.0523	3.9583
G55-3	40.9633	0.0401	0.0034	4.0476	3.9385
A1-1	13.4741	0.0214	0.0012	6.0467	15.7122
A1-2	7.0968	0.0164	0.0006	8.9877	36.5020
A1-3	32.0093	0.0318	0.0049	3.4521	2.3615
A1-4	43.6434	0.0429	0.0036	4.0530	3.9630
A1-5	39.1090	0.0393	0.0042	3.6391	2.8217
CS1-1	12.9714	0.0227	0.0017	6.6517	18.2136
CS1-2	16.2535	0.0245	0.0018	5.7011	12.0847
CS1-3	28.4174	0.0373	0.0029	4.9206	6.7659
CS1-4	20.4252	0.0268	0.0021	4.9221	6.7808
CS1-5	25.1049	0.0309	0.0025	4.9290	6.8475
SW1-1	4.2921	0.0134	0.0005	12.3459	46.1250
SW1-2	22.1421	0.0308	0.0021	5.2434	10.4812
SW1-3	25.8305	0.0268	0.0039	3.6213	2.8385
SW1-4	28.5299	0.0271	0.0030	3.4026	2.2826

while the average SSA and BJH pore volume of the Mahantango is 8.98 m^2/g and 0.018 cm^3/g, respectively. Overall, the pore volume does not change as significantly as pore surface area, mainly because smaller pores (pore size smaller than 5 nm) does not contribute very much to pore volume, but make a significant difference in the pore surface area (Song et al., in prep). The smallest SSA measured is 4.2921 m^2/g from sample SW1-1, and the greatest SSA is 43.6434 m^2/g from sample A1-4. The micropore volume is represented by the t-plot volume. The Mahantango samples have smaller micropore volumes, while Marcellus samples has larger micropore volumes (Table 4).

Pore size distributions reveal that the TOC influences the pore structure, especially micropore volume and SSA (Fig. 5). The least organic-rich sample (SW1-1, TOC: 0.41%) shows almost no micro porosity. With slightly higher TOC (0.65–2.24%), the rest of Mahantango samples exhibit similar characteristics, but with higher amount of micropores as TOC increases (Fig. 5A). The majority of the pores in Mahantango Formation are larger than 10 nm. The organic-rich Marcellus samples (TOC: 2.33–7.88%) demonstrate greater pore space, specifically micropores. Sample G55-2, G55-3, A1-3, A1-4, and A1-5 exhibit similar PSD, with the majority of pores between 4 and 10 nm. These 5 samples also show the largest SSA. Low thermal maturity Marcellus samples SW1-3 and SW1-4 show limited mesopore occurrence compared with other organic-rich samples (Fig. 5).

4. Discussion

4.1. Relationship between pore structure parameters

Shale samples with smaller pores have larger specific surface area and pore volume. Fig. 6 illustrates a general negative relationship between specific surface area and pore size (average pore width, median pore size). Pore volume and pore size show the same negative correlation (Table 4, Fig. 6). The porosity value in this research as determined by the GRI method shows a negative correlation between porosity and pore size (Fig. 7). All samples show an increase in pore volume and surface area with decreasing pore size.

4.2. Relationships between pore structure and TOC

The influences of organic matter on the pore structure are demonstrated in Fig. 8. The Marcellus Shale demonstrates a significantly greater adsorbed and free-gas storage capacity, (SSA and pore volume respectively) compared to the Mahantango Formation. The least organic-rich sample SW1-1 (TOC 0.41%) shows the least SSA and pore volume, and the largest pore size (Table 4). In this sample with negligible organic matter, most of the pores are hosted by non-organic minerals. Previous workers attribute increasing SSA and pore volume with increasing TOC and the development of OM-hosted pores [13,30,49]. Indeed, our results yield a good correlation between TOC and SSA and pore volume (Fig. 8), and porosity (Fig. 9A). The increase of TOC also is

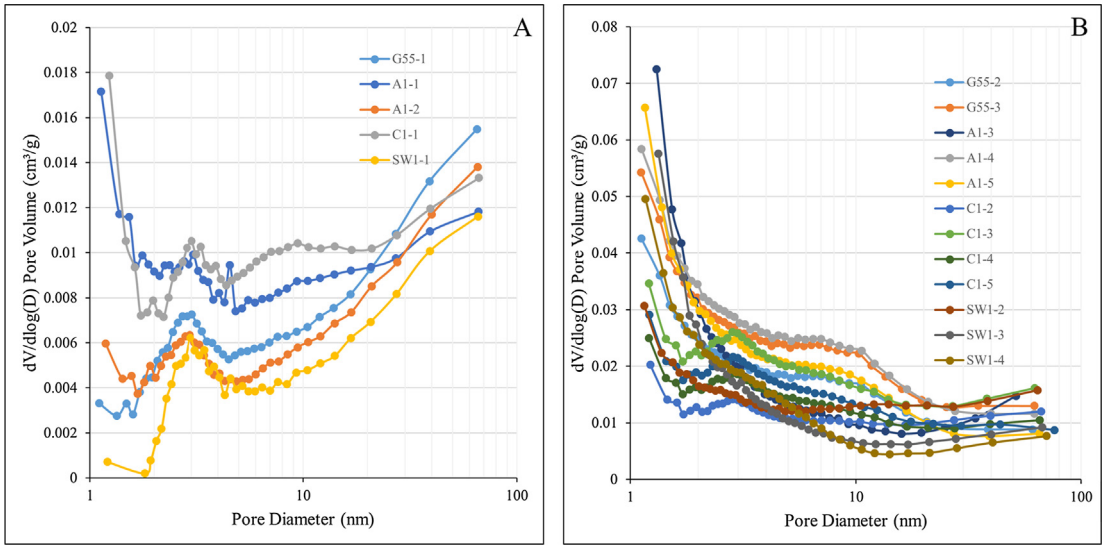

Fig. 5. Pore size distribution of samples from Mahantango and Marcellus Formations, A: Mahantango, B: Marcellus.

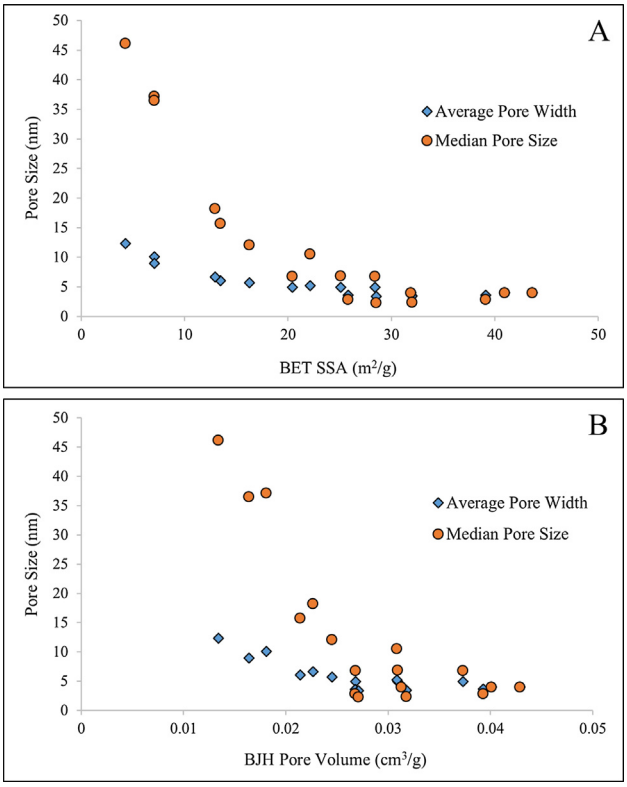

Fig. 6. Relationship between pore structure parameters.

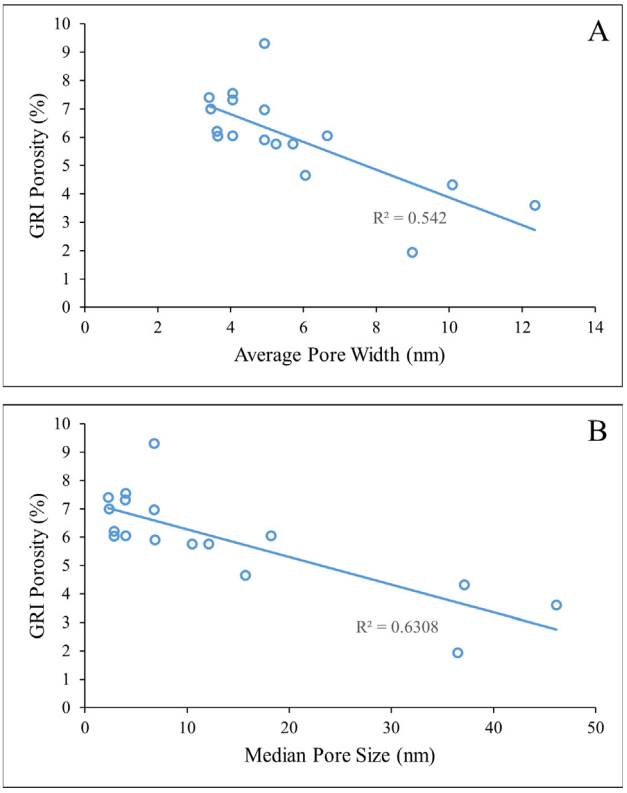

Fig. 7. Relationships between GRI porosity and (A) average pore width, and (B) median pore size.

related to a decrease in pore size (Fig. 9B). This argument agrees with previous research on porosity development in other shale units [13,42,49–53]. At lower TOC content, all the samples show a similar range in SSA and pore volume. As TOC increases, there is more variance in the storage capacity at higher TOC. Samples from well G55 and A1 show a better storage capacity than SW1 and CS1.

4.3. Relationships between pore structure and minerals

No correlation was observed between carbonate or quartz content and SSA. Fig. 10 shows a negative correlation between clay content and the storage capacity. Pure clay minerals have been found to have large specific surface area [54]. For illite, the BET SSA is usually on the order of 100 m^2/g, and the BET SSA of kaolinite and chlorite typically stays on the order of 10 m^2/g [3]. However, clay-rich samples of the Marcellus Shale and Mahantango Formation do not demonstrate an increase in contribution to SSA and pore volume (Table 2, Fig. 3). This phenomenon may be attributed to the accessibility of the pore space. This result agrees with Milliken et al., 2013's research [30] that the Marcellus Shale is an *organic matter-hosted pore system*. Organic matter shows the most significant control on the storage capacity than minerals.

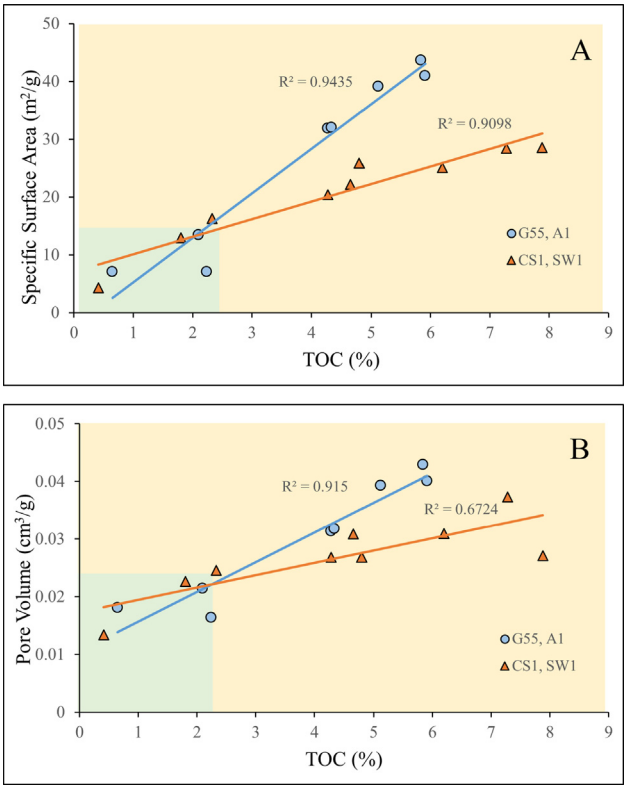

Fig. 8. Relationship between specific surface area, pore volume, and TOC. Data points in green shadow are from Mahanntango Fm., while yellow shadow covers the Marcellus samples. (For interpretation of the references to colour in this figure legend, the reader is referred to the web version of this article.)

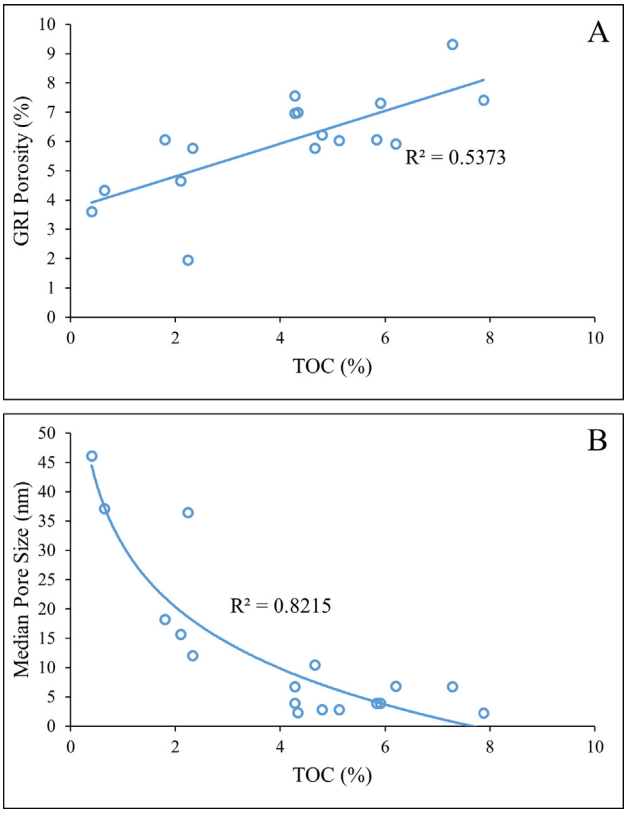

Fig. 9. Relationship between TOC and (A) GRI porosity, and (B) median pore size.

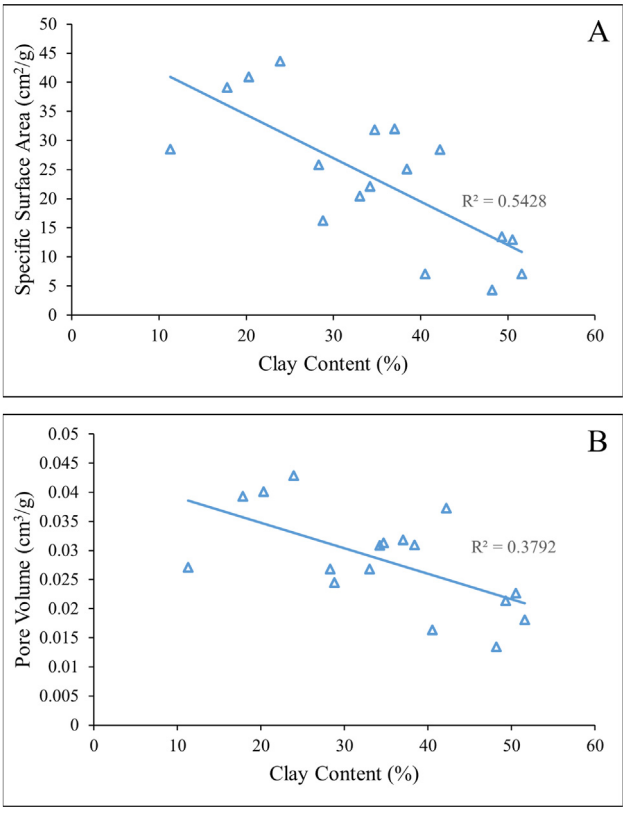

Fig. 10. Relationships between clay content and (A) specific surface area, and (B) pore volume.

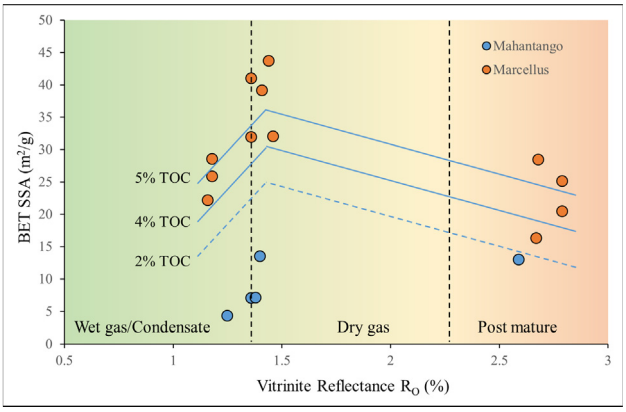

Fig. 11. Relationship between thermal maturity (represented by vitrinite reflectance) and specific surface area.

4.4. The relationship between thermal maturity and pore structure

Thermal maturity also plays a very important but complex role in evaluating the storage capacity of shales [5,7,10,30,35,55–59]. Fig. 11 shows the results of SSA involve with respect to vitrinite reflectance. The samples cover a thermal maturity ranging from the late oil window (well SW1), to the dry gas window (G55, A1), ending in the post-mature zone (CS1). Regardless of thermal maturity, we notice a significant strong positive correlation (R^2 = 0.9098 or 0.9435) between TOC and SSA in both Marcellue Shale and Mahantango samples (Fig. 8A). Given a similar TOC level, samples in the dry gas window shows the highest SSA, and samples from the post-mature zone shows the least. Our observation supports the ideas that porosity is altered during maturation, and organic matter is largely responsible for porosity changes because of the transformation of its kerogen and bitumen into hydrocarbons and

other liquids. Further, at post-mature thermal maturities, there is a reduction in storage capacity.

5. Conclusions

The SSA, pore volume, and pore size were measured for four different wells penetrating the Mahantango and Marcellus formations from West Virginia and Pennsylvania. Samples cover a wide range of thermal maturity and hydrocarbon generation windows from 1.16 to 2.79% R_o. Furthermore, samples have a wide range of TOC, clay content and type. The following conclusions based on the results in this study are:

1. The presence of organic matter in shale strongly enhances the storage capacity by increasing the SSA and pore volume, which represents sorption storage capacity and free-gas storage capacity;
2. As TOC increases, average and median pore sizes decrease;
3. Carbonate and quartz do not show any correlation with porosity, SSA, or pore volume;
4. Organic matter has more significant influence on SSA and pore volume than clay content. A negative correlation is found between clay content and specific surface area and pore volume. We suspect that pore space within clay minerals is inaccessible.
5. The development of organic matter pores is altered during thermal maturation. Samples in the dry gas window show highest SSA and pore volume, while those samples from the post-mature zone show a reduced range of storage capacity under the same TOC level.

Acknowledgements

We thank Dr. Konstantinos Sierros, Derrick Banerjee, and Flexible Electronics for Sustainable Technologies (FEST) lab in the Mechanical and Aerospace Engineering Department of WVU for providing the Micromeritics ASAP 2020 instrument. We appreciate Chloe Wonnell and Vikas Agrawal for conducting the SRA TOC test. We also thank Dr. Eric Suuberg and the reviewers, whose constructive input greatly improved this manuscript. The research undertaken in this study was funded through the U. S. DoE National Energy Technology Lab as part of their Marcellus Shale Energy and Environmental Laboratory (MSEEL) (DOE Award No.: DE-FE0024297).

References

[1] Kuila U, Prasad M. Specific surface area and pore-size distribution in clays and shales. Geophys Prospect 2013;61:341–62. https://doi.org/10.1111/1365-2478.12028.
[2] Saidian M, Kuila U, Prasad M, Barraza SR, Godinez LJ, Alcanntar-Lopez L. A comparison of measurement techniques for porosity and pore size distribution in shales (Mudrocks): a case study of Haynesville, Eastern European Silurian, Niobrara, and Monterey Formations. Imaging Unconv. Reserv. Pore Syst. AAPG Mem 2016;112:89–114.
[3] Saidian M, Godinez LJ, Prasad M. Effect of clay and organic matter on nitrogen adsorption specific surface area and cation exchange capacity in shales (Mudrocks). Annu Logging Symp 2015;56:1–16.
[4] Wang G, Ju Y, Yan Z, Li Q. Pore structure characteristics of coal-bearing shale using fluid invasion methods: a case study in the Huainan-Huaibei Coalfield in China. Mar Pet Geol 2015;62:1–13. https://doi.org/10.1016/j.marpetgeo.2015.01.001.
[5] Bai B, Elgmati M, Zhang H, Wei M. Rock characterization of Fayetteville shale gas plays. Fuel 2013;105:645–52. https://doi.org/10.1016/j.fuel.2012.09.043.
[6] Nelson PH. Pore-throat sizes in sandstones, tight sandstones, and shales. Am Assoc Pet Geol Bull 2009;3:329–40. https://doi.org/10.1306/10240808059.
[7] Mastalerz M, Schimmelmann A, Drobniak A, Chen Y. Porosity of DEVONIAN and Mississippian New Albany Shale across a maturation gradient: Insights from organic petrology', gas adsorption, and mercury intrusion. Am Assoc Pet Geol Bull 2013;97:1621–43. https://doi.org/10.130/04011312194.
[8] Javadpour F. Nanopores and apparent permeability of gas flow in Mudrocks (Shales and Siltstone). J Can Pet Technol 2009;48:16–21.
[9] Sondergeld CH, Newsham KE, Comisky JT, Rice MC, Rai CS. SPE 131768: petrophysical considerations in evaluating and producing shale gas resources. Pittsburgh, PA: SPE Unconv. Gas Conf; 2010.
[10] Ross DJK, Marc Bustin R. Impact of mass balance calculations on adsorption capacities in microporous shale gas reservoirs. Fuel 2007;86:2696–706. https://doi.org/10.1016/j.fuel.2007.02.036.
[11] Ross DJK, Bustin RM. Characterizing the shale gas resource potential of Devonian-Mississippian strata in the Western Canada sedimentary basin: application of an integrated formation evaluation. Am Assoc Pet Geol Bull 2008;92:87–125. https://doi.org/10.1306/09040707048.
[12] Chalmers GRL, Marc Bustin R. On the effects of petrographic composition on coalbed methane sorption. Int J Coal Geol 2007;69:288–304. https://doi.org/10.1016/j.coal.2006.06.002.
[13] Chalmers GRL, Ross DJK, Bustin RM. Geological controls on matrix permeability of Devonian Gas Shales in the Horn River and Liard basins, northeastern British Columbia, Canada. Int J Coal Geol 2012;103:120–31. https://doi.org/10.1016/j.coal.2012.05.006.
[14] Ross DJK, Bustin RM. The importance of shale composition and pore structure upon gas storage potential of shale gas reservoirs. Mar Pet Geol 2009;26:916–27. https://doi.org/10.1016/j.marpetgeo.2008.06.004.
[15] Ettensohn FR, Lierman TR. Large-scale tectonic controls on the origin of Paleozoic Dark-shale source-rock basins: examples from the Appalachian Foreland Basin, Eastern United States. Am Assoc Pet Geol Bull 2012;100:95–124. https://doi.org/10.1306/13351549M1003529.
[16] EIA. Marcellus Shale Play Geology Review. 2017.
[17] Friedman GM, Johnson KG. The Devonian Catskill Deltaic complex of New York, type example of a "Tectonic Delta Complex". Houst Geol Soc Deltas Their Geol Framework 1966:171–88.
[18] Faill RT. The Acadian Orogeny and the Catskill Delta. Catskill Delta. Geol Soc Am Spec Pap 1985;201:15–38.
[19] Ettensohn FR. The Catskill Delta complex and the Acadian Orogeny: a model. Catskill Delta. Geol Soc Am Spec Pap 1985;201:39–49.
[20] Lash GG, Engelder T. Thickness trends and sequence stratigraphy of the Middle Devonian Marcellus Formation, Appalachian Basin: implications for Acadian foreland basin evolution. Am Assoc Pet Geol Bull 2011;95:61–103. https://doi.org/10.1306/06301009150.
[21] Lash GG, Blood DR. Organic matter accumulation, redox, and diagenetic history of the Marcellus Formation, southwestern Pennsylvania, Appalachian basin. Mar Pet Geol 2014;57:244–63. https://doi.org/10.1016/j.marpetgeo.2014.06.001.
[22] Blood R, Lash G, Bridges L. Biogenic Silica in the Devonian Shale Succession of the Appalachian Basin, USA. AAPG Annu Conv Exhib 2013:211–25. 50864.
[23] Sageman BB, Murphy AE, Werne JP, Ver Straeten CA, Hollander DJ, Lyons TW. A tale of shales: The relative roles of production, decomposition, and dilution in the accumulation of organic-rich strata, Middle-Upper Devonian, Appalachian basin. Chem Geol 2003;195:229–73. https://doi.org/10.1016/S0009-2541(02)00397-2.
[24] Zagorski WA, Wrightstone GR, Bowman DC. The Appalachian Basin Marcellus gas play: its history of development, geologic controls on production, and future potential as a world-class reservoir. AAPG Mem 97 Shale Reserv Resour 21st Century 2012:172–200. https://doi.org/10.1306/13321465M973491.
[25] Soeder DJ. The development of natural gas from the marcellus shale. Boulder, Colorado: The Geological Society of Amarica; 2017.
[26] Soeder DJ. Eastern Devonian Gas Shale. 1988.
[27] Davies DK, Bryant WR, Vessell RK, Burkett PJ, Directorate OS, Oceanographic N, et al. Porosities, permeabilities, and microfabrics of Devonian shales. Microstruct. Fine-grained sediments from mud to shale. Springer; 1991. p. 109–19.
[28] Luffel DL, Guidry FK. New Core Analysis Methods for Measuring Reservoir Rock Properties of Devonian Shale. In: SPE Annu. Tech. Conf. Exhib., 1992, p. 1184–90. doi:10.2118/20571-PA.
[29] Strapoć D, Mastalerz M, Schimmelmann A, Drobniak A, Hasenmueller NR. Geochemical constraints on the origin and volume of gas in the New Albany Shale (Devonian-Mississippian), eastern Illinois Basin. Am Assoc Pet Geol Bull 2010;94:1713–40. https://doi.org/10.1306/06301009197.
[30] Milliken KL, Rudnicki M, Awwiller DN, Zhang T. Organic matter-hosted pore system, Marcellus Formation (Devonian), Pennsylvania. Am Assoc Pet Geol Bull 2013;97:177–200. https://doi.org/10.1306/07231212O48.
[31] Gu X, Cole DR, Rother G, Mildner DFR, Brantley SL. Pores in Marcellus shale: a neutron scattering and FIB-SEM study. Energy Fuels 2015;29:1295–308. https://doi.org/10.1021/acs.energyfuels.5b00033.
[32] Jarvie DM, Hill RJ, Ruble TE, Pollastro RM. Unconventional shale-gas systems: the Mississippian Barnett Shale of north-central Texas as one model for thermogenic shale-gas assessment. Am Assoc Pet Geol Bull 2007;91:475–99. https://doi.org/10.1306/12190606068.
[33] Loucks RG, Reed RM, Ruppel SC, Jarvie DM. Morphology, genesis, and distribution of nanometer-scale pores in siliceous mudstones of the Mississippian Barnett Shale. J Sediment Res 2009;79:848–61. https://doi.org/10.2110/jsr.2009.092.
[34] Bernard S, Wirth R, Schreiber A, Schulz H, Hors B. Formation of nanoporous pyrobitumen residues during maturation of the Barnett Shale (Fort Worth Basin). Int J Coal Geol 2012;103:3–11. https://doi.org/10.1016/j.coal.2012.04.010.
[35] Curtis ME, Ambrose RJ. Investigation of the relationship between organic porosity and thermal maturity in the Marcellus Shale. In: SPE Conf., vol. SPE 144370, 2011, p. 4. doi:10.2118/144370-ms.
[36] Pommer M, Milliken K. Pore types and pore-size distributions across thermal maturity, Eagle Ford Formation, southern Texas. Am Assoc Pet Geol Bull 2015;99:1713–44. https://doi.org/10.1306/03051514151.
[37] Song L, Paronish T, Agrawal V, Hupp B, Sharma S. Depositional environment and impact on pore structure and gas storage potential of Middle Devonian Organic Rich Shale, Northeastern West Virginia, Appalachian Basin. Austin, Texas, USA: Unconv. Resour. Technol. Conf.; 2017. doi:10.15530/urtec-2017-2667397.
[38] Wang G, Carr TR. Organic-rich marcellus shale lithofacies modeling and distribution pattern analysis in the appalachian basin. Am Assoc Pet Geol Bull 2013;97:2173–205. https://doi.org/10.1306/05141312135.

[39] Chen R, Sharma S, Bank T, Soeder D, Eastman H. Comparison of isotopic and geochemical characteristics of sediments from a gas- and liquids-prone wells in Marcellus Shale from Appalachian Basin, West Virginia. Appl Geochem 2015;60:59–71. https://doi.org/10.1016/j.apgeochem.2015.01.001.
[40] Chen R, Sharma S. Role of alternating redox conditions in the formation of organic-rich interval in the Middle Devonian Marcellus Shale, Appalachian Basin, USA. Palaeogeogr Palaeoclimatol Palaeoecol 2016;446:85–97. https://doi.org/10.1016/j.palaeo.2016.01.016.
[41] Chen R, Sharma S. Linking the Acadian Orogeny with organic-rich black shale deposition: evidence from the Marcellus Shale. Mar Pet Geol 2017;79:149–58. https://doi.org/10.1016/j.marpetgeo.2016.11.005.
[42] Clarkson CR, Wood JM, Burgis SE, Aquino SD, Freeman M. Nanopore-structure analysis and permeability predictions for a tight gas siltstone reservoir by use of low-pressure adsorption and mercury-intrusion techniques. SPE Reserv Eval Eng 2012;15:648–61. https://doi.org/10.2118/155537-PA.
[43] Brunauer S, Emmett PH, Teller E. Adsorption of Gases in Multimolecular Layers. J Am Chem Soc 1938;60:309–19. citeulike-article-id:4074706\rdoi: 10.1021/ja01269a023.
[44] Barrett EP, Joyner LG, Halenda PP. The determination of pore volume and area distributions in porous substances. I. Computations from nitrogen isotherms. J Am Chem Soc 1951;73:373–80. https://doi.org/10.1021/ja01145a126.
[45] Sing K. The use of nitrogen adsorption for the characterisation of porous materials. Colloids Surf, A 2001;187–188:3–9. https://doi.org/10.1016/S0927-7757(01)00612-4.
[46] Sing KSW, Everett DH, Haul RAW, Moscou L, Pierotti RA, Rouquérol J, et al. Reporting physisorption data for gas/solid systems with special reference to the determination of surface area and porosity. Pure Appl Chem 1982;57:603–19. https://doi.org/10.1351/pac198557040603.
[47] Thommes M, Kaneko K, Neimark AV, Olivier JP, Rodriguez-Reinoso F, Rouquerol J, et al. Physisorption of gases, with special reference to the evaluation of surface area and pore size distribution (IUPAC Technical Report). Pure Appl Chem 2015;87:1051–69. https://doi.org/10.1515/pac-2014-1117.
[48] Sing KSW, Williams RT. Physisorption hysteresis loops and the characterization of nanoporous materials. Adsorpt Sci Technol 2004;22:773–82. https://doi.org/10.1260/0263617053499032.
[49] Loucks RG, Reed RM, Ruppel SC, Hammes U. Spectrum of pore types and networks in mudrocks and a descriptive classification for matrix-related mudrock pores. Am Assoc Pet Geol Bull 2012;96:1071–98. https://doi.org/10.1306/08171111061.
[50] Bustin RM, Bustin A, Ross D, Chalmers G, Murthy V, Laxmi C, et al. Shale gas opportunities and challenges. Search Discov Artic 2009. 40382.c.
[51] Yu W, Sepehrnoori K, Patzek TW. Modeling gas adsorption in Marcellus shale with Langmuir and BET isotherms. SPE J 2016;21:589–600. https://doi.org/10.2118/170801-PA.
[52] Tian H, Pan L, Xiao X, Wilkins RWT, Meng Z, Huang B. A preliminary study on the pore characterization of Lower Silurian black shales in the Chuandong Thrust Fold Belt, southwestern China using low pressure N2 adsorption and FE-SEM methods. Mar Pet Geol 2013;48:8–19. https://doi.org/10.1016/j.marpetgeo.2013.07.008.
[53] Mosher K, He J, Liu Y, Rupp E, Wilcox J. Molecular simulation of methane adsorption in micro- and mesoporous carbons with applications to coal and gas shale systems. Int J Coal Geol 2013;109–110:36–44. https://doi.org/10.1016/j.coal.2013.01.001.
[54] Saidian M, Godinez LJ, Prasad M. Effect of clay and organic matter on nitrogen adsorption speci fi c surface area and cation exchange capacity in shales (mudrocks). J Nat Gas Sci Eng 2016;33:1095–106. https://doi.org/10.1016/j.jngse.2016.05.064.
[55] Modica CJ, Lapierre SG. Estimation of kerogen porosity in source rocks as a function of thermal transformation: example from the Mowry Shale in the Powder River Basin of Wyoming. Am Assoc Pet Geol Bull 2012;1:87–108. https://doi.org/10.1306/04111110201.
[56] Löhr SC, Baruch ET, Hall PA, Kennedy MJ. Is organic pore development in gas shales influenced by the primary porosity and structure of thermally immature organic matter? Org Geochem 2015;87:119–32. https://doi.org/10.1016/j.orggeochem.2015.07.010.
[57] Zhang T, Ellis GS, Ruppel SC, Milliken K, Yang R. Organic geochemistry effect of organic-matter type and thermal maturity on methane adsorption in shale-gas systems. Org Geochem 2012;47:120–31. https://doi.org/10.1016/j.orggeochem.2012.03.012.
[58] Schieber J. SEM observations on ion-milled samples of Devonian Black Shales from Indiana and New York: the petrographic context of multiple pore types. Electron Microsc Shale Hydrocarb Reserv AAPG Mem 2013;102:153–72. https://doi.org/10.1306/13391711M1023589.
[59] Romero-Sarmiento MF, Rouzaud JN, Bernard S, Deldicque D, Thomas M, Littke R. Evolution of Barnett Shale organic carbon structure and nanostructure with increasing maturation. Org Geochem 2014;71:7–16. https://doi.org/10.1016/j.orggeochem.2014.03.008.